DELAYED STALL MODELLING OF THE ROTATING BLADES

Horia DUMITRESCU, Vladimir CARDOŞ

"Gh. Mihoc-C. Iacob" Institute of Statistical Mathematics and Applied Mathematics, Bucharest, Romania
E-mail: horiadumitrescu@yahoo.com

Most aerodynamic design tools for horizontal-axial wind turbines are based on the blade-element momentum theory. Due to the nature of this theory, the design tools need 2-D steady sectional lift and drag curves as an input. In practice, flow over a wind turbine rotor blade is neither two-dimensional nor steady, and is affected by rotation. Pioneering experiments have identified a consequence: at inboard rotor blade sections stall is delayed. This so-called Himmmelskamp effect gives a larger lift than predicted and, as a result, a higher power and loading than expected. Consequently, an aerodynamic model is needed to explain and predict sectional lift and drag under rotating conditions. In this paper development and validation against the computed and measured results, of such a model is described.

Key words: Three-dimensional boundary layer; Boundary layer separation; Rotational effects.

1. INTRODUCTION

Wind turbine blade sections can operate with stall at low tip speed ratios and can undergo delayed stall [1], characterized by strong differences between the measured performances and predictions based on 2-D airfoil characteristics in stall conditions. Thus predicting blade loads and the power output during stall is fundamental to the improved design of the fixed-speed stall-regulated turbines.

Modeling of delayed stall through the numerical solution of the Navier-Stokes equations with CFD techniques has shown some recent success [2–3] and has become increasingly feasible with the increase in computational power. CFD solutions are, however, still computationally very expensive and are basically prohibitive for the routine engineering analyses of wind turbines. In addition, there are numerous issues such as rotational turbulence modeling that still need to be understood. In the absence of less approximate and cost-effective solutions, researchers have used various semi-empirical models to represent stall-delay. The advantage of using these models is their relative simplicity and low computational expense. Nevertheless, no practically useful method for accurate predicting this phenomenon was generated.

The present work aims at giving a clearer interpretation of the three-dimensional effects on the rotor blade sections in stall using the available numerical and experimental results. Then, the main contributions for the rise of the delayed stall phenomenon are discussed and assessed.

2. SURVEY OF PREVIOUS RESULTS

The local air velocity relative to a rotor blade consists of free-wind velocity V_w defined as the wind speed if there were no rotor present, that due to the blade motion $\Omega_b r$ and the wake induced velocities (not important for present analysis). Wind turbine blade sections can operate in two main regimes depending on the amount of rotation parameter defined as the ratio of wind velocity to the local tangential velocity $V_w / \Omega_b r$. If the rotation parameter is less than unity along the entire span the flow is mostly two-dimensional and attached, while for rotation parameter greater than unity the flow is neither two-dimensional nor steady, and is affected by rotation. Here, the inboard flow with enhanced rotation produces, along the suction side of the rotor blade sections, a leading edge separation bubble which remains attached through high angles of attack.

For the prior stall regime $V_w/\Omega_b r \leq 1$, the relative velocity at a specific position on the blade is written as

$$U_{rel} = \left(V_w^2 + \Omega_b^2 r^2\right)^{1/2},$$ (1)

where the effective incoming flow velocity is simply composed of the free-flow velocity and the induction velocity from rotor. Therefore, the incoming flow field results from a weak interaction between two different flows: one axial and other rotational.

The theoretical description of the flow of air is based on the potential flow model that complies with the radial independence principle of flow effects, i.e. the radial component of velocity is dependent only upon the 2-D velocity potential and it is independent of the span. In the prior-stall state the following findings are important for the understanding of the flow effects in the sequel:

- the main parameter of influence of the weak interaction flow is the radius by local chord ratio r/c;
- the shape of the chordwise pressure coefficient distribution normalized by the maximum pressure coefficient $\left|C_{pm}\right|$ and the corresponding pressure gradients along the upper surface are not really affected by r/c, i.e. the pressure parameter $\left|C_{pm}\right|$ is dependent only the airfoil shape, incidence and Reynolds number [4, 5];
- the suction side distribution of the pressure coefficients moves slightly towards lower levels as r/c decreases [4, 5];
- the separation point location moves slightly downstream towards the trailing edge as r/c decreases [4, 5];
- the Coriolis force induced in the chordwise direction by rotation is the main contribution of the favorable effect in separation delaying, resulting in slight lift increasing, [4, 5].

These features that are attributable to rotation usually are neglected in the traditional BEM model, with lift and drag forces determined from 2-D measurements. The model reduces the complexity of the problem by an order of magnitude yielding reliable results for the local forces and the overall torque in the proximity of the design point, at high tip speed ratios. But, the wind turbine blade sections often operate with stall at low tip speed ratios and can undergo delayed stall phenomenon on the inner part of span. As the wind velocity increases the inboard regions of the blades are stalled having $V_w/\Omega_b r > 1$ for much of their operational time. Thus predicting blade loads and the power output during stall is fundamental to the improved design of wind turbines.

The post-stall regime is characterized by a strong nonlinear interaction between the high wind speed and the rotational flow induced by a constant-speed rotor and now the relative velocity can be written as

$$U_{rel} = \Omega_b \left(\frac{V_w^2}{\Omega_b^2 r^2} + 1\right)^{1/2} r = \Omega_f \left(\frac{r}{c}, \frac{V_w}{\Omega_b r}\right) r,$$ (2)

a form that suggests an outer rotational flow with angular velocity higher than that of the constant-speed rotor.

Numerical and experimental studies [2–3, 6], have been directed towards understanding the complex 3-D flow physics that are associated with the post-stall region. Nevertheless, little detailed information concerning the understanding the basic fluid mechanics of inboard stall-delay is still rather unclear. Some features associated with the flow physics responsible for rotational stall delay come from [7]. These recent findings are consistent with the numerical studies [2, 3] and they can be summarized as follows:

- two non-dimensional parameters $V_w/\Omega_b r$ and r/c are important for further understanding of the strong interaction flow;
- at high wind velocities the suction side of the inner half-rotor behaves like a disk rotating slower than the outer flow, $\Omega_b < \Omega_f$ [7];
- the enhanced rotational outer flow acts at the root area of the blade as a vortex that produces a sucking effect and radial mass flux towards the rotation center;

- the pressure coefficient distributions are gradually smoothed, as $V_w / \Omega_b r$ increases and the pressure coefficient with no suction spike moves rapidly towards pressure distributions with no suction spike at leading edge;
- at high angles of attack the sucking effect produces leading edge separation bubbles, attached, instead of the usual leading edge separation (stall), resulting mainly in stall delaying and higher lift and drag as compared with 2-D stall.

A theoretical description of the strong interaction flow must be able to capture both the enhanced rotational flow effect and the high-lift effect of the airfoils at high angle of attack. Also, an important result is that the midspan rapid lift-drag rise governs the peak power of rotor, but the sequence of these aerodynamic events as yet is not well understood.
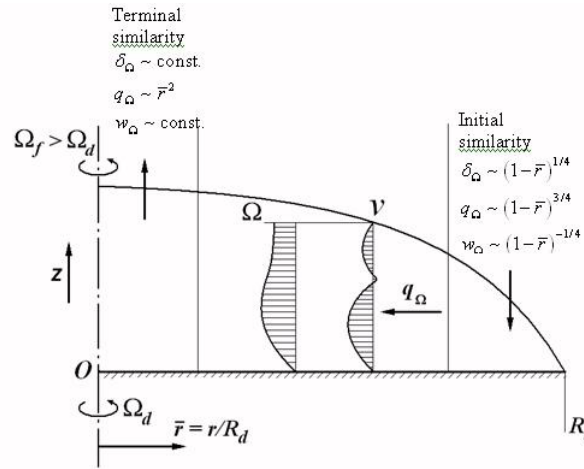
3. MODELLING OF 3-D AND ROTATIONAL EFFECTS

Fig. 1 – Boundary layer on a rotating disk slower than the outer flow (vortex-induced sucking effect).

Boundary layer on a finite disk (in a faster rotating flow). The rotating disk in an axial flow is a generalization of the rotating disk case which depends not only the number Reynolds $\mathrm{Re} = \Omega_d R_d^2 / \nu$, but also on the rotation parameter $V_\infty / \Omega_d R_d$. The strong nonlinear interaction between the rotating outer flow and the boundary layer developing on the disk produces a radial inflow accompanied by an axial inflow near the edge of the disk and an axial outflow in the central core (Fig. 1). In order to analysis the enhanced rotation by high axial velocities (strong winds) consider the axisymmetric laminar rotating flow of a viscous incompressible fluid over a disk of radius R_d (Fig. 1). The angular velocity of the disk Ω_d is constant and that of the fluid far away from the disk Ω_f may be an arbitrary function of the radius r, provided it is stable, i.e. $\mathrm{d}\left(\Omega_f r^2\right)/\mathrm{d}r > 0$ (for potential vortex rotation $\Omega_f r^2 = \mathrm{const.}$) and near the axis the outer flow behaves locally like a rigid body rotation, i.e. $r \to 0 : \mathrm{d}\Omega_f / \mathrm{d}r \to 0, \Omega_f \to \Omega_{f0}$ (finite). The fluid is assumed to be an ideal gas with constant properties and zero bulk viscosity and the flow is laminar. We use the following nondimensional quantities defined for an inertial system of cylindrical coordinates: $(\bar{r}, \bar{z}) = (r, z)/R_d, (\bar{u}, \bar{v}, \bar{w}) = (u, v, w)/\Omega_d R_d \left(\Omega_d < \Omega_f\right)$. The equation of state is $p/\rho = \mathrm{const.}$ The nondimensional parameter of the flow field is the Ekman number, $E = \dfrac{\nu}{\Omega_d R^2}$, where $\nu = \dfrac{\mu}{\rho}$ is the kinematical viscosity. It is also assumed that the Ekman number is small enough so that boundary layer approximations are valid and the boundary layer equations write as

$$\frac{\partial (ru)}{\partial r} + \frac{\partial (rw)}{\partial z} = 0 ,$$

(3)

$$\frac{\partial\left(u^2\right)}{\partial r}+\frac{u^2-v^2}{r}+\frac{\partial\left(uw\right)}{\partial z}=-\frac{1}{\rho}\frac{\partial p}{\partial r}+\nu\frac{\partial^2 u}{\partial z^2}\,, \tag{4}$$

$$\frac{\partial\left(uv\right)}{\partial r}+\frac{2uv}{r}+\frac{\partial\left(vw\right)}{\partial z}=\nu\frac{\partial^2 v}{\partial z^2}\,, \tag{5}$$

with $\frac{\partial p}{\partial z}=0$.

The boundary conditions at the surface of the disk are $z=0:u=w=0,v=\Omega_d r$. The conditions at the edge of the boundary layer and the pressure distribution are given by the outer flow, for which we assume that the radial velocity is negligible and the azimuthally velocity is a function of radius only. The outer flow radial momentum equation is then $\Omega_f^2 r=\frac{1}{\rho}\frac{dp}{dr}$ and the pressure in the outer flow is

$$\frac{\Delta p}{\rho}=\frac{p\left(R_d\right)-p\left(r\right)}{\rho}=\int_r^{R_d}\Omega_f^2 r dr\,. \tag{6}$$

The conditions at the edge of the boundary layer thus read: $z=\delta_\Omega:u=0,\Omega=\frac{v}{r}=\Omega_f$.

Now, we define a boundary coordinate $\eta=zE^{-1/2}/\delta_\Omega$ based on the boundary layer thickness $\delta_\Omega\left(r\right)=\delta_E E^{1/2}$ and assume radial and angular velocity profiles which satisfy the boundary conditions at the disk surface and the smoothness requirements at the edge of the boundary layer:

$$u=U\left(r\right)f'\left(\eta\right),f'\left(0\right)=0,f'\left(1\right)=0,f''\left(1\right)=0\,, \tag{7}$$

$$\frac{\Omega-\Omega_d}{\Omega_f-\Omega_d}=g\left(\eta\right),g\left(0\right)=0,g\left(1\right)=1,g'\left(1\right)=0\,. \tag{8}$$

The radial mass flux in the boundary layer is

$$q=\int_0^{\delta_E}\rho r u d\left(zE^{-1/2}\right)=\rho r\delta_E E U f\left(1\right). \tag{9}$$

Integrating (3)–(5) with the profiles (7), (8), and using the nondimensional quantities we have the radial and azimuthally momentum integral equations for two unknowns: the radial mass flow $\overline{q}\left(\overline{r}\right)$ and the boundary layer thickness $\overline{\delta}_E\left(\overline{r}\right)$

$$\frac{d}{d\overline{r}}\left[\overline{q}\left(\overline{\Omega}_f-1\right)\right]-\lambda_1\overline{q}\frac{d\left(\overline{\Omega}_f-1\right)}{d\overline{r}}-\frac{2\overline{q}}{\overline{r}}\lambda_1\left[\frac{\lambda_1-1}{\lambda_1}\left(\overline{\Omega}_f-1\right)+1\right]=\frac{\lambda_1 c_1\overline{r}}{\overline{\delta}_E}\left(\overline{\Omega}_f-1\right), \tag{10}$$

$$\lambda_2\frac{d}{d\overline{r}}\left[\frac{\overline{q}^2}{\overline{\delta}_E\overline{r}^2}\right]+\lambda_2\frac{\overline{q}^2}{\overline{\delta}_E\overline{r}^3}+\overline{\delta}_E\overline{r}\left[\lambda_3\left(\overline{\Omega}_f-1\right)^2+\lambda_4\left(\overline{\Omega}_f-1\right)\right]=-\frac{c_2\overline{q}}{\overline{\delta}_E^2\overline{r}}\,. \tag{11}$$

Here $\overline{\Omega}_f=\Omega_f/\Omega_d$ and the parameters $\lambda_1,\lambda_2,\lambda_3,\lambda_4,c_1,c_2$ are forms parameters[7].

Boundary layer an rotating blades. There are two rules that synthesize to a great extent the results known so far. The first rule states that: "The chordwise pressure coefficient distribution along the upper surface and normalized by its maximum value is not dependent on the ratio r/c in prior-stall flow". The second rule which governs the post-stall flow states that: "The normalized chordwise pressure coefficient distribution on the upper surface at a given inboard location is strongly dependent on the parameter $V_w/\Omega_b r$, but preserves the integrated coefficient until the inboard separation bubble is broken down and the flow is stalled". In other words, the lift coefficient on the blade section at high angle of attack can be found

from the loading on the local airfoil and incidence at the same station by integrating the known inviscid solution. This rule which assumes a principle of pressure redistribution is sketched as is shown in Fig. 2.
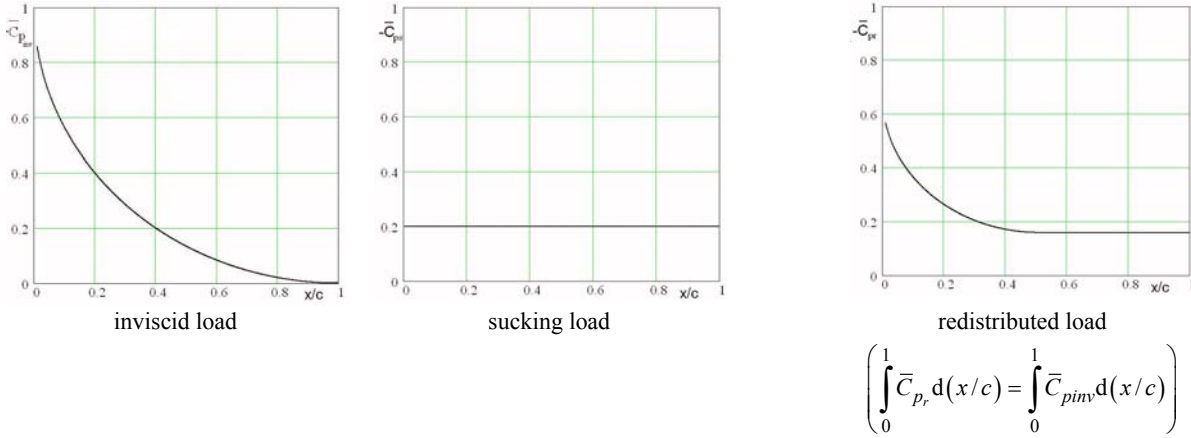

inviscid load   sucking load   redistributed load

$$\left(\int_0^1 \bar{C}_{pr}\,\mathrm{d}(x/c) = \int_0^1 \bar{C}_{pinv}\mathrm{d}(x/c) \right)$$

Fig. 2 – The rule of the suction pressure with superimposed rotation (in normalized plan).

To illustrate these considerations concerning the blade section characteristics a three-dimensional boundary-layer model is used. The incompressible three-dimensional boundary layer equations are written in integral form in cylindrical coordinate system (θ, r, z) which rotates with the blade at constant rotational speed Ω_b (Fig. 3). θ denotes the peripheral, r the radial (blade spanwise) and z the axial (wind) direction.
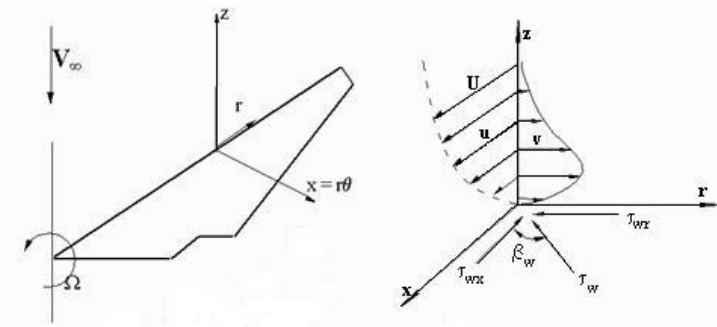

Fig. 3 – Cylindrical coordinate system fixed to the rotating blade: nature of chordwise (u) and spanwise (v) velocity profiles.

The governing equations have been developed in [8]. For simplicity the equations are presented here in their laminar form. The momentum integral equation in $x = r\theta$ (inviscid streamline) and r directions in the rotating orthogonal coordinate system is given, respectively by

$$\frac{\partial \delta_x}{\partial x} + \frac{1}{U_e}\frac{\partial U_e}{\partial x} + \frac{\partial \delta_{2xr}}{\partial r} - \frac{\zeta}{U_e}\left(2\delta_{2xr} + \delta_{1r}\right) - 2\frac{\Omega_z}{U_e}\delta_{1r} = \frac{1}{2}C_{fx}, \tag{12}$$

$$\frac{\partial\left(\delta_{2xr} + \delta_{1r}\right)}{\partial x} + \frac{2}{U_e}\frac{\partial U_e}{\partial x}\left(\delta_{2xr} + \delta_{1r}\right) + \frac{\partial \delta_{2xr}}{\partial r} + \frac{1}{U_e}\frac{\partial U_e}{\partial r}\left(\delta_{2r} + \delta_{1x} + \delta_{2x}\right) - $$
$$-\frac{\zeta}{U_e}\left(\delta_{2r} - \delta_{1x} - \delta_{2x}\right) + 2\frac{\Omega_z}{U_e}\delta_{1x} = \frac{1}{2}C_{fr}, \tag{13}$$

where U_e is the inviscid freestream velocity, $\zeta = \left(\nabla \times \mathbf{V_e}\right)_z = -\frac{1}{r}\frac{\partial}{\partial r}\left(rU_e\right) = -2\Omega_z$, $\Omega_z = \Omega_b$ and $\left(C_{fx}, C_{fr}\right)$ are the laminar skin friction coefficient components. Equations (12) and (13) can be written in

terms of the three parameters: the boundary layer thickness $\dfrac{\delta^2}{\nu}$, the Pohlhausen shape parameter

$\Lambda = \dfrac{\delta^2}{\nu} \dfrac{\partial U_e}{\partial x}$, and the limiting streamline parameter ε_w [8].

The inviscid flow distribution along the upper surface of the blade needed to complete the above boundary-layer description is given according to the radial independence principle

$$U_e = U_r U_{2D}, V_e \cong 0,\qquad (14)$$

where $U_r = \left(V_w^2 + \Omega_b^2 r^2\right)^{1/2}$ is the reference velocity at a point on blade and the nondimensional velocity $U_{2D} = \sqrt{1 - C_p}$ depends only on the local aerodynamic field at a certain radial station. The aerodynamic loading over the chord C_p is prescribed by means of an one-parameter distribution family

$$C_p = \left|C_{p_m}\right| \left(\sqrt{\dfrac{x}{c}\left(2 - \dfrac{x}{c}\right)} - 1 \right),\qquad (15)$$

where the maximum pressure coefficient $\left|C_{p_m}\right|$ is a parameter depending only on the local aerodynamic field: the airfoil shape, incidence and Reynolds number. This pressure distribution family ranges a large area from the prior-stall pressure distributions, values of $\left|C_{p_m}\right| = 2 - 5$, until the post-stall pressure distributions with $\left|C_{p_m}\right| = 6 - 10$.

Since the primary objective of the present study is to investigate the sucking effect of the leading-edge suction pressure on the boundary-layer separation, the proposed distribution (15) is an excellent demonstrator for the physical mechanism of the operation in the stalled inboard regions of the blades.
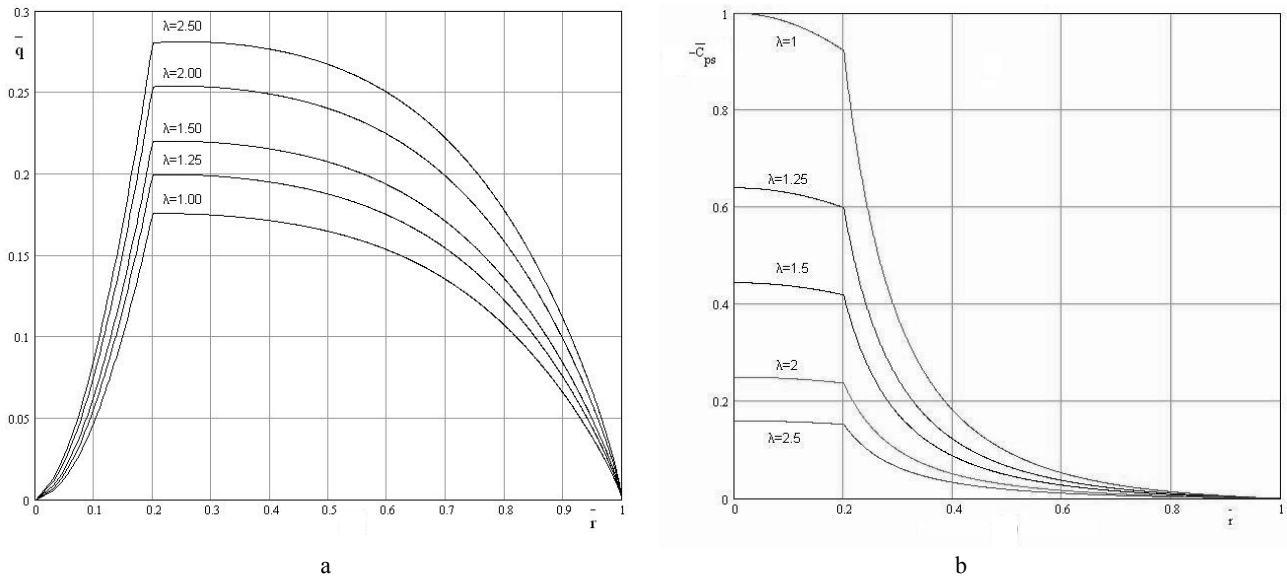
4. NUMERICAL RESULTS

a

b

Fig. 4 – Sucking characteristics for a disk rotating slower than the outer flow: a) mass flow rate; b) sucking pressure.

The results obtained by numerical integration of (10) and (11) with variable $\overline{\Omega}_f$ for the outer Rankine vortex flow and various parameters $\dfrac{V_w}{\Omega_d R_d}$ or $\dfrac{1}{\lambda}$ are presented in Fig. 4, where the pressure coefficient shown is defined as

$$C_{p_s} = -\frac{\Delta p}{\rho/2\left(V_\infty + \Omega_d^2 r^2\right)}, \tag{16}$$

or in normalized plan $\overline{C}_{p_s} = C_{p_s}/C_{p_h}$, where C_{p_h} is the reference pressure on the hub of the rotor.
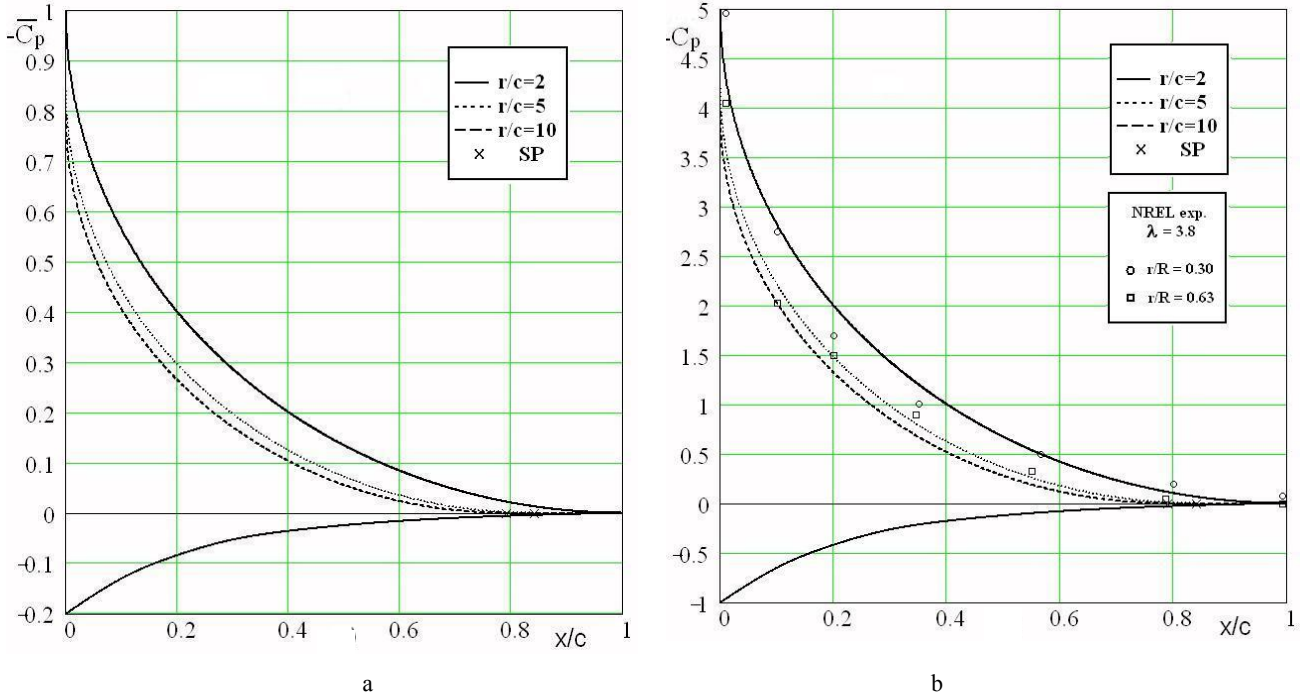

a

b

Fig. 5 – Influence of the r/c ratio on the pressure and the separation point location (SP) for $\dfrac{V_w}{\Omega_b r} < 1$: a) normalized plan; b) physical plan ($\left|C_{p_m}\right| = 5$).

Figure 5 illustrates the rule governing the flow field around the airfoils in the prior-stall running $(\lambda > 2.5)$ and the contribution of Coriolis force to the delay in boundary layer separating. The relationships between the maximum pressure coefficient $\left|C_{p_m}\right|$ and the separation position $(x/c)_s$ in terms of the ratio r/c are shown in both normalized and physical plan. The Coriolis force acts in the chordwise direction as a favorable pressure gradient resulting in slightly increasing of $\left|C_{p_m}\right|$ and $(x/c)_s$ as r/c decreases.

The second rule governing the post-stall running $\left(\lambda \leq 2.5 \text{ and } \dfrac{V_w}{\Omega_b r} \geq 1\right)$ is better understood considering Fig. 6 where the redistributed suction pressure coefficient C_{p_r}, and the separation/reattachment position, $(x/c)_s/(x/c)_r$, are plotted against the sucking pressure coefficient C_{p_s} for $\left|C_{p_m}\right| = 10$ and r/c = 2. Increasing the air sucking along the suction side of the airfoil one notes considerable changes between the leading edge region with a sharp suction peak, and the region with smooth pressure variations over the chord showing a flattening of the pressure distribution with practically no suction surface pressure gradient.
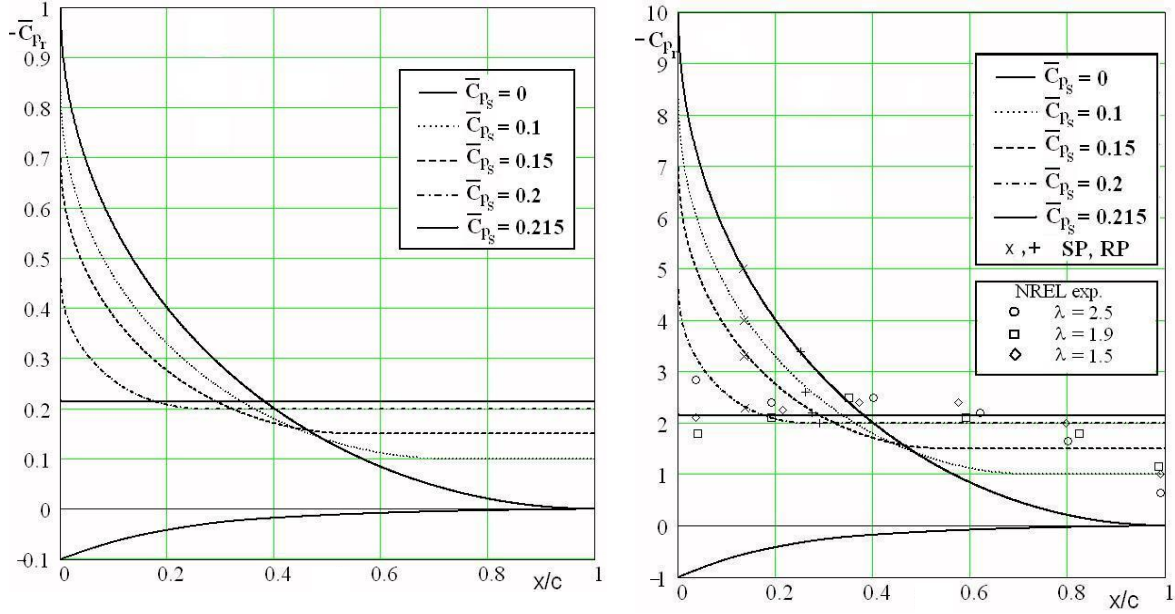
Fig. 6 – Influence of the C_{p_s} sucking effect on the pressure distribution for $\dfrac{V_w}{\Omega_b r} > 1$: a) normalized plan;

b) physical plan ($\left| C_{p_m} \right| = 10, r/c = 2$).

The comparisons of measured [6], computed [2, 3] and modeled pressure distributions are shown for the higher wind speeds (15 (λ=2.5), 20 (λ=1.9) and 25 (λ=1.5) m/s) at the spanwise section $r/R = 0.30$ ($r/c = 2$) that correspond to $\overline{C}_{p_s} = 0.2 - 0.215$ (Fig. 6b).

The stall-delay behaviour and its explanation is well captured. The spanwise section $r/R = 0.47$ ($r/c \cong 4$) which is stalled for these cases shows a surprisingly good agreement with the assumption $r_b / R \cong (1+\lambda)^{-1}$ for the location of the bubble burst. Furthermore, the representation from Fig. 6a shows a physical limitation in the amount of the possible pressure in the sucking effect so that pressure distributions for r/c = 2 have no suction surface pressure gradient $\displaystyle\int_0^1 \overline{C}_{pinv} \mathrm{d}(x/c) = \int_0^1 \overline{C}_{p_s,b} \mathrm{d}(x/c) = 0.215$ .Still, these pressure distributions attain C_p maximum of -2.15 that remains virtually constant for any sucking increase [6].

4. CONCLUSIONS

Using concepts of boundary layer theory we have studied the chordwise velocity boundary-layer superimposed with the radial angular velocity (Ekman) boundary-layer which occurs at the high wind-speed flow. The major conclusions are follows:

1. The rotational flow over the suction surface of the rotor, which is characterized by the rotation parameter $V_w / \Omega_b r$, has an important effect upon the boundary-layer state and the flow field structure on the wind turbine blade surface. For less than unity values $V_w / \Omega_b r$ <1 the prior-stall flow (high tip speed ratios) remains largely attached to the surface of the blade. In contrast, for grater than unity values $V_w / \Omega_b r$ >1 (low tip speed ratios) the post-stall flow along most of the span occurs associated with separation on the suction surface of the blade.

2. The post-stall flow manifests itself through inboard delayed stall with leading-edge separation bubbles and outboard stall aft the bubble burst. The flow aft of the separation line is largely in the radial direction, towards the tip of the blade. The interface flow between the inboard delayed stall-flow and the outboard stall-flow is associated with the bubble burst which is generally located at midspan. A better approximation is proposed by the empirical formula $r_b / R \cong (1+\lambda)^{-1}$.

3. Two main contributions can be equally attributed to the rise of the stall-delay phenomenon: one is the speedy rotational flow induced at the hub which produces a sucking effect, resulting in suction pressure reducing/smoothing at the leading-edge, and the other one is the Coriolis force which acts in the chordwise direction as a favorable pressure gradient tending to the alleviate separation downstream towards the trailing edge. Concerning the centrifugal forces this effect known as pumping effect is largely produced aft of the bubble burst resulting in spanwise flow.

REFERENCES

1. TANGLER, J. L., *Insight into wind turbine stall and post-stall aerodynamics*, Wind Energy **7**, pp. 247–260, 2004.
2. SØRENSEN, N. N., MICHELSEN, J. A., SCHRECK, S., *Navier-Stokes predictions of the NREL PhaseVI Rotor, in the NASA Ames 80 ft×120 ft wind tunnel*, Wind Energy **5**, pp. 151–169, 2002.
3. FLETCHER, T. M., BROWN, R. E., KIM, D. H., KWON, O. J., *Predicting wind turbine blade loads using vorticity transport and RANS methodologies*, European Wind Energy Conference & Exhibition, Parc Channot, Marseille, France, 1–10, 2009.
4. CHAVIAROPOULOS, P. K., HANSEN, M. O. L., *Investigating three-dimensional and rotational effects on wind turbine blades by means of a quasi-3-D Navier-Stokes solver*, Journal of Fluids Engineering, **122**, pp. 330–336, 2000.
5. SHEN, W. Z., SØRENSEN, J. N*., Quasi-3-D Navier-Stokes model for rotating airfoil*, Journal of Computational Physics, **150**, pp. 518–548, 1999.
6. SCHRECK, S., ROBINSON, M., *Rotational augmentation of horizontal axis wind turbine blade aerodynamic response*, Wind Energy **5**, pp. 133–150, 2002.
7. DUMITRESCU, H., CARDOŞ, V., *Inboard stall delay for wind turbine blades*, European Wind Energy Conference & Exhibition, 16-19 March, Parc Chanot, Marseille, 2009.
8. DUMITRESCU, H., CARDOŞ, V., *Inboard boundary layer state on wind turbine blades*, ZAMM, **89**, *3*, pp. 163–173, 2009.